AIP Advances

Role of hydrogen carrier gas on the growth of few layer hexagonal boron nitrides by metal-organic chemical vapor deposition

Cite as: AIP Advances **7**, 045116 (2017); https://doi.org/10.1063/1.4982029
Submitted: 03 January 2017 . Accepted: 09 April 2017 . Published Online: 17 April 2017

Dong Yeong Kim, Nam Han , Hokyeong Jeong, Jaewon Kim, Sunyong Hwang, and Jong Kyu Kim

COLLECTIONS

EP This paper was selected as an Editor's Pick

ARTICLES YOU MAY BE INTERESTED IN

Layer number dependent optical properties of multilayer hexagonal BN epilayers
Applied Physics Letters **110**, 092102 (2017); https://doi.org/10.1063/1.4977425

Probing carbon impurities in hexagonal boron nitride epilayers
Applied Physics Letters **110**, 182107 (2017); https://doi.org/10.1063/1.4982647

Direct growth of nanocrystalline hexagonal boron nitride films on dielectric substrates
Applied Physics Letters **106**, 101901 (2015); https://doi.org/10.1063/1.4914474

© 2017 Author(s).

Role of hydrogen carrier gas on the growth of few layer hexagonal boron nitrides by metal-organic chemical vapor deposition

Dong Yeong Kim, Nam Han, Hokyeong Jeong, Jaewon Kim, Sunyong Hwang, and Jong Kyu Kim[a]
Department of Materials Science and Engineering, Pohang University of Science and Technology (POSTECH), Pohang 37673, South Korea

(Received 3 January 2017; accepted 9 April 2017; published online 17 April 2017)

Few layer hexagonal boron nitride (h-BN) films were grown on 2-inch sapphire substrates by using metal-organic chemical vapor deposition (MOCVD) with two different carrier gases, hydrogen (H_2) and nitrogen (N_2). Structural, optical and electrical properties of the MOCVD-grown h-BN films were systematically investigated by various spectroscopic analyses and electrical conduction measurement. Based on the experimental findings including narrower X-ray photoelectron spectra, reduced intensity of the shoulder peaks in near edge X-ray absorption fine structure spectra, and decreased electrical conduction by more than three orders of magnitude when H_2 carrier gas is employed, it was concluded that H_2 has an advantage over N_2 as the carrier gas for MOCVD growth of h-BN which is attributed to the healing of crystalline defects by etching and regrowth processes occurring under the pulsed source-injection mode. © *2017 Author(s). All article content, except where otherwise noted, is licensed under a Creative Commons Attribution (CC BY) license (http://creativecommons.org/licenses/by/4.0/).* [http://dx.doi.org/10.1063/1.4982029]

Hexagonal boron nitride (h-BN) is a two-dimensional (2D) layered material with honeycomb lattice like graphene but composed of alternating boron and nitrogen atoms.[1–3] Despite of the same atomic structure with graphene which has zero bandgap energy, it has wide bandgap energy of approximately 6 eV.[4–7] Synthesis of h-BN has attracted a great attention for its promising potential applications in 2D (opto-) electronics as an ideal insulting substrate[8,9] gate dielectrics,[10] and tunneling barriers since it is an atomically thin layered insulator with clean surface without dangling bonds and charged defects. It can be also utilized as a surface passivation layer because of its chemical inertness and high oxidization resistance.[11] In addition, h-BN was also proposed as an active material for an ultraviolet light emitter replacing the conventional Hg-vapor-based lamps or AlGaN-based ultraviolet light-emitting diodes (LEDs) due to its strong light-matter interaction originating from the 2D nature.[4,5,12–14]

In the industrial perspective, wafer-scale growth of 2D materials becomes one of the most critical issues. Metal-organic chemical vapor deposition (MOCVD) has been proposed as a very promising solution to achieve wafer-scale growth of h-BN on sapphire or other substrates, since Y. Kobayashi *et al.*, demonstrated MOCVD-grown h-BN as a releasing layer for transferring the GaN-based LED epitaxial structure grown on the h-BN onto foreign flexible substrates.[15–17] Recently, Q. S. Paduano *et al*, reported self-terminating effect in MOCVD growth of h-BN[18] and investigated effects of growth parameters including reactor pressure, and V/III ratio, defined as molar flow ratio between NH_3 and triethylborane (TEB) which are source of nitrogen and boron respectively, on thickness of MOCVD-grown h-BN.[19] X. Z. Du *et al.*, studied effects of V/III ratio on the luminescence properties of MOCVD-grown h-BN and succeeded in synthesizing h-BN epitaxial layers without emission at around 300 nm which is known to be from impurities such as C and O.[14]

[a]Corresponding author, e-mails: kimjk@postech.ac.kr

 © Author(s) 2017

Meanwhile, carrier gas is also an important factor determining properties of semiconductors grown by chemical vapor deposition (CVD) method including MOCVD growth, especially for atomically thin and flat 2D materials since it strongly affects the gas phase chemical reaction influencing growth rate, surface morphology and crystallinity of the grown film. There are several reports on the evolution of h-BN crystal under different gas ambient with and without nitrogen (N), in which the carrier gas is considered as a source of N atoms.[20,21] M. Chubarov *et al.*, claimed that pure hydrogen gas (H_2) ambient seems to be necessary for growth of rhombohedral BN layers by a hot wall MOCVD at the temperature of 1500 °C based on X-ray diffraction pattern.[22] However, there is a lack of systematic studies on the effect of carrier gas on the structural properties of MOCVD-grown h-BN, and explanation why H_2 carrier gas is more suitable for the growth of sp^2-hybridized h-BN film.

In this work, we synthesized few-layer h-BN films grown with two different carrier gases, H_2 and nitrogen gas (N_2) for understanding the role of carrier gas in the MOCVD growth of h-BN. Structural properties of two h-BN films were investigated by the various spectroscopic techniques including X-ray photoelectron spectroscopy (XPS) and near-edge X-ray absorption fine structure (NEXAFS) spectroscopy. In addition, electrical conduction in MOCVD-grown h-BN films were also measured for comparing crystallinity because shallow defects of h-BN can influence the electrical conduction by generating charge carriers.[23] We found that the h-BN film grown with N_2 carrier gas contains more defects comparing to the film grown with H_2 carrier gas resulting in the peak broadening in the XPS spectra, and defect-related shoulder peaks observed in the NEXAFS spectra. In addition, the electrical conduction was remarkably larger through the h-BN film grown with N_2 carrier gas. Based on the experimental observations, it was concluded that H_2 has advantages over N_2 as a carrier gas for h-BN MOCVD growth, and the possible reasons why the crystallinity of h-BN can be improved when H_2 is used as a carrier gas are discussed.

h-BN films were grown on 2-inch sapphire substrates by a commercial MOCVD system with capability of 11×2-inch wafers at 1050 °C and reactor pressure of 30 mbar. A pulsed source-injection mode, in which TEB and NH_3 were injected at different times with an interruption time, i.e., no injection of sources in between, was employed for alleviating undesired pre-reactions between gas-phase sources.[24,25] A single pulse cycle was composed of 4 steps; injection of 10 sccm TEB for 5 seconds, interruption for 2 seconds, injection of 8,000 sccm NH_3 for 4 seconds, and interruption for 2 seconds, and the total number of the pulse cycle was 100. In order to investigate the role of the carrier gas on MOCVD growth of h-BN films, two h-BN films were synthesized by using different carrier gases, H_2 and N_2, while all the other growth parameters were kept same.

For the structural characterization, atomic force microscopy (AFM), Raman spectroscopy, X-ray reflectance (XRR), optical absorption spectroscopies were performed for the as-grown samples. XPS and NEXAFS measurements were carried out at 4D beam line in Pohang Accelerator Laboratory for the transferred h-BN films onto a conductive silicon substrate by using PMMA-assisted transferring method. PMMA was spun on the grown h-BN film, followed by the delamination of the h-BN film from the sapphire substrate which was easily done by immersing it to the diluted hydrofluoric acid solution. For the electrical conduction measurement, rectangular $100 \times 50\ \mu m^2$ Ti/Au (20/150 nm) metal contacts with spacing of 3.5 μm were fabricated by using conventional photolithography and electron beam evaporation of Ti and Au, followed by rapid thermal annealing at 800 °C for 1 minute under N_2 ambient. The current-voltage measurement was performed in the vacuum condition (pressure < 10 mTorr) at the elevated temperature of 500 K in a chamber probe station system.

Figure 1 shows the structural and optical properties of two h-BN films grown with H_2 and N_2 carrier gas, respectively. Raman scattering at around 1370 cm^{-1} is observed from both films which corresponds to the E_{2g} vibration mode of h-BN[7] as shown in Fig. 1(a). Figure 1(b) shows the optical absorption spectra from the films. The optical bandgap energies obtained from the absorption edge are identical, 5.92 eV, for the two films despite of a little difference in the absorbance peak position and a long-wavelength absorption tail observed from the h-BN film grown with N_2 carrier gas. Thickness of the grown films is estimated to be 2.66 nm and 1.55 nm for the h-BN grown with H_2 and N_2 carrier gas, respectively, by fitting the XRR spectrum shown in Fig. 1(c). The both h-BN films consist of only a few atomic layers which is due to self-terminating effect occurring at low pressure and high V/III

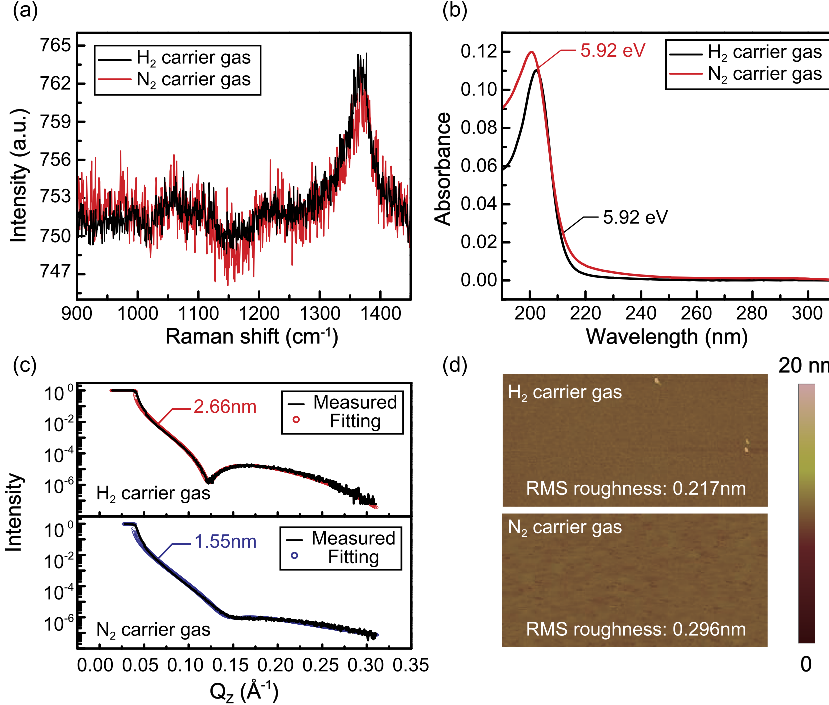

FIG. 1. (a) Raman spectrum, (b) optical absorption spectrum and the optical bandgap energy, (c) the measured and fitted X-ray reflectance, and (d) surface morphology obtained by AFM of the h-BN film grown with H_2 carrier and that with N_2 carrier gas.

ratio growth conditions,[18,19] but the films have a different saturated thickness depending on the carrier gas. It is also experimentally observed that thickness of the sample is no longer increasing when the total pulse cycle number is increased further (not shown here). The surface roughness is investigated by AFM. The both films have very smooth surface with root-mean-square(RMS) roughness smaller than 0.3 nm in the scanning area of 5 um $\times$ 5 um, but the h-BN film grown with H_2 carrier gas shows slightly smoother surface than that grown with N_2 carrier gas as seen in Fig. 1(d).

Figure 2(a) and (b) are the B 1s and N 1s core-level XPS spectra of the h-BN films, respectively. Open circles indicate measured data and the red lines show the fitted data. The binding energy of the B 1s core level is 190.9 eV for both films. However, there is an additional peak in B 1s XPS spectrum from the h-BN film grown with N_2 carrier gas at 192.6 eV. This peak may originate from the sp^3-hybridized boron atoms because their binding energy is typically higher than sp^2-hydrydized boron atoms.[26] In addition, the FWHM of the B 1s main peak becomes larger from 1.80 eV to 1.88 eV when N_2 is used as the carrier gas instead of H_2. Since peak broadening is related to the numbers of contributing chemical bonding,[27] boron atoms in the h-BN film grown with N_2 carrier gas possess

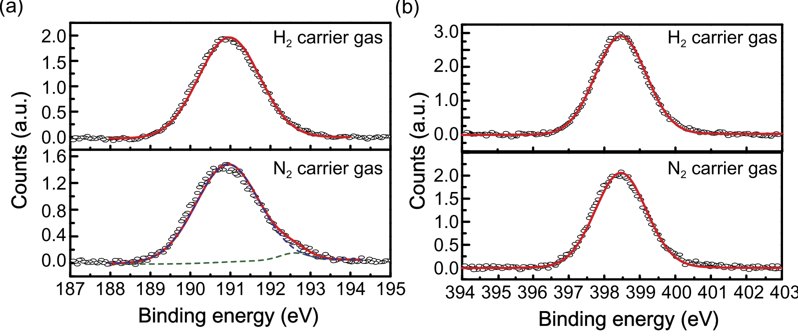

FIG. 2. Core level XPS spectrum of (a) B 1s and (b) N 1s for the h-BN films grown with different carrier gas.

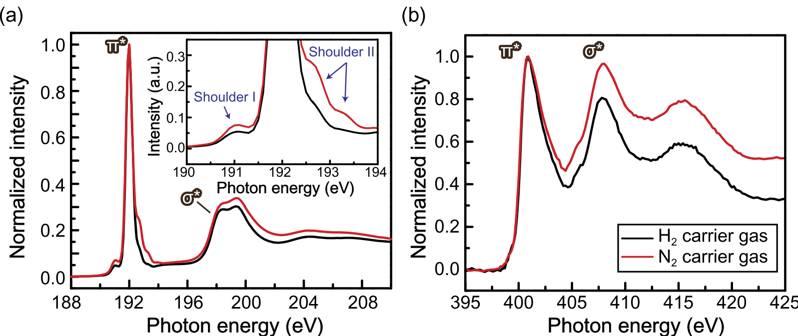

FIG. 3. (a) B K-edge NEXAFS spectrum (inset) enlarged graph showing the vicinity of shoulder peak and (b) N K-edge NEXAFS spectrum of the MOCVD-grown h-BN films with different carrier gases.

more defective chemical bonding states comparing to that grown with H_2 carrier gas. Meanwhile, the binding energy of the N 1s core level is 398.4 eV for the both h-BN films and the FWHM is also almost identical.

In order to further investigate structural properties of MOCVD-grown h-BN films depending on the carrier gas, NEXAFS spectroscopy is carried out by using the synchrotron X-ray source. Figure 3(a) is the normalized B K-edge NEXAFS spectra of the two h-BN films. Peaks at 192.0 eV originate from the transition between B 1s core level and π* anti-bonding orbital state of the sp^2-hybridized boron atoms. Double peaks at around 199.0 eV are due to the transition between B 1s state and σ* anti-bonding states.[28–30] The NEXAFS spectrum supports that both BN films are composed of sp^2-hybridized boron atoms, thus, h-BN phase. An important feature in the B K-edge spectra is the shoulders at both lower- and higher-energy of the π* peak as clearly shown in inset of the Fig. 3(a). The shoulders with higher energy (Shoulder II in inset) at around 193.0 eV is reported as the nitrogen vacancy-related peak and the shoulder with lower energy (Shoulder I in inset) at around 190.1 eV is related to the boron atoms bonded to the four neighbor nitrogen atoms.[28] Consequently, both the shoulders indicate the existence of defects and atomic disorders in the h-BN layers. When N_2 is used as the carrier gas instead of H_2, both shoulder peaks in the B K-edge become more prominent, indicating that the crystallinity of grown h-BN film becomes deteriorated. Figure 3(b) is the normalized N K-edge NEXAFS spectra of the h-BN films, indicating that there is no significant change in shape and position of peaks regardless of the carrier gas. Peak at 399.7 eV and 406.8 eV correspond to π* and σ* states, respectively, which also indicates existence of sp^2-hydridized nitrogen atoms.[28–30]

Figure 4(a) is the NEXAFS B K-edge spectra around the π* peak at various X-ray incident angles. Based on the transition theory, optical transition probability is determined by wavefunctions of initial and final states and polarization of the incident light.[31] In the case of NEXAFS B K-edge spectrum which originates from the transition from 1s state to π* anti-bonding state, the initial 1s

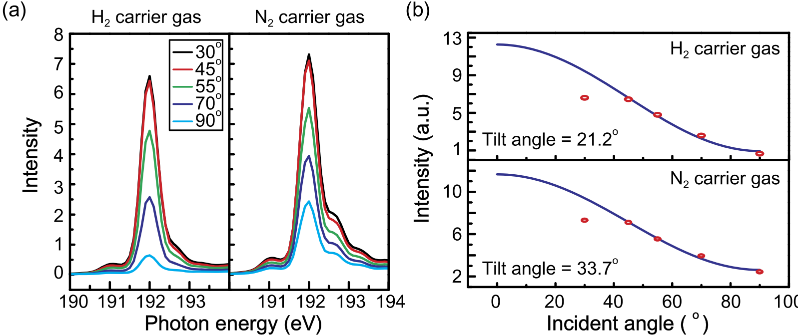

FIG. 4. (a) Angle-dependent B K-edge NEXAF spectrum of the h-BN films grown with different carrier gases. (b) Measured intensity of the π* peak as a function of X-ray incident angle (open red circles) and the fitted data (blue line) for calculating average tilt angle.

state has even-symmetry wavefunction. Therefore, this optical transition is simply determined by the relation between the wavefunction of π* anti-bonding orbital, which is vertically aligned to the h-BN atomic plane, and the polarization direction of the incident X-ray controlled by the incident angle of the linearly polarized synchrotron source. For the sp^2-hybridized layered materials, X-ray absorption from 1s core-level to π* state decreases as X-ray incident angle increases, and it is expressed by the following equation.[32]

$$I = C \cdot \frac{P}{3}\left\{1 + \frac{1}{2}\left(3\cos^2\theta - 1\right)\left(3\cos^2\alpha - 1\right)\right\} + \frac{(1-P)}{2}\sin^2\alpha \tag{1}$$

where, C is a constant, P is the degree of polarization, which is set to be 0.85 for the equipment used in this experiment, θ is the polarization angle of the incident beam with respect to the surface normal direction, and α is the average tilt angle of the planar geometry.

The intensity of the π* peak in B K-edge spectrum decreases as θ increases for the both h-BN films as expected. However, there is difference in intensity reduction ratio with increasing the X-ray incident angle between two films due to the difference in the average tilt angle α that indicates how well the atomic planes are aligned in the in-plane direction. The average tilt angles obtained by using Eq. 1 are 21.2° and 33.7° for h-BN films grown with H_2 carrier gas and N_2 carrier gas, respectively, as shown in Fig. 4(b). The average tilt angle is strongly related to the atomic defects existing in layered films because defects can generate chemical bonding deviating from the in-plane direction, and anti-bonding orbitals formed not in the direction perpendicular to the in-plane but in an oblique direction. Therefore, the larger average tilt angle obtained from the h-BN grown with N_2 carrier gas compared to that obtained from the h-BN grown with H_2 carrier gas is consistent with the previously presented results showing improved crystallinity of the h-BN film when H_2 is used.

Electrical conduction was measured for both samples because it can be strongly affected by defects in h-BN films. Figure 5 shows the electrical conduction in the h-BN films, and the measured data (symbols) is well matched with the calculated ones (solid line) following the Poole-Frenkel type conduction behavior expressed by,

$$J = q\mu N_C E \cdot \exp\left[\frac{-q\left(\phi_T - \sqrt{qE/\pi\varepsilon_i\varepsilon_0}\right)}{kT}\right] \tag{2}$$

where, q is element charge, μ is drift mobility, N_C is the density of states in the conduction band, E is the electric field, ϕ_T is trap-level, ε_i and ε_0 are the dielectric constant in dielectric film and vacuum, respectively, and kT is the thermal energy.[33] The Poole-Frenkel type conduction behavior indicates that there are traps which can be ionized under a strong electric field. Despite of the same Poole-Frenkel type conduction behavior for both the h-BN films, there is huge difference in conduction level. The current density in the h-BN film grown with N_2 carrier gas is more than three orders of magnitude higher than that in the h-BN grown with H_2 carrier gas. Such a significant difference in the electrical conduction level is associated with the large amount of defects acting as donors or acceptors in the h-BN film. Carrier type in MOCVD-grown h-BN film was not experimentally determined, but

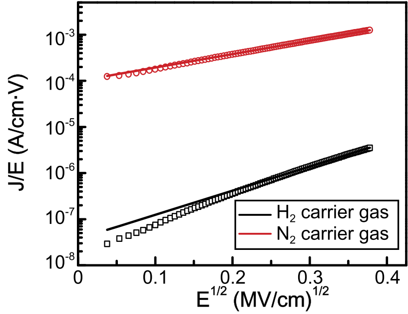

FIG. 5. Poole-Frenkel type electrical conduction in h-BN films grown with different carrier gases.

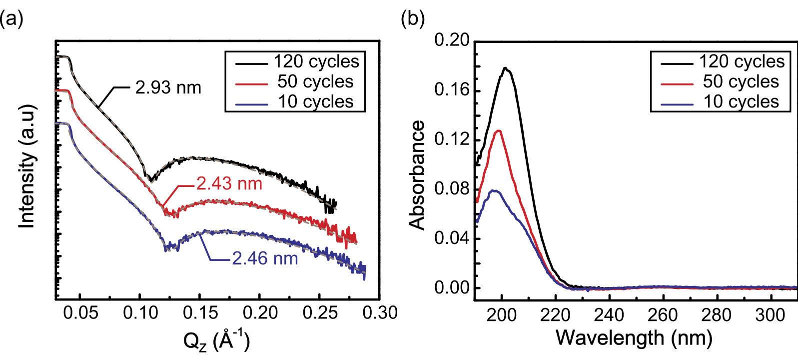

FIG. 6. (a) X-ray reflectance, and (b) optical absorption spectrum of the h-BN films grown for different pulse cycles of 10, 50, 120 when H_2 carrier gas is used.

it may be electron because of nitrogen vacancy, which can act as a donor by making shallow defect levels,[34] observed in the NEXAFS B K-edge spectrum.

Based on the experimental observations, it can be concluded that H_2 has advantages over N_2 as a carrier gas for the growth of h-BN by MOCVD, which can be elucidated by etching and regrowth process occurring under the pulsed source-injection mode employed in this study. The etching of the grown III-nitride semiconductors by H_2 at an elevated temperature is well-known phenomenon.[35,36] Defective regions with point defects or grain boundaries of the grown h-BN film can be preferentially etched during interruption steps of source-injection cycle when only H_2 carrier gas is injected to the reactor. Then, new h-BN crystal can be regrown at the etched region for TEB or NH_3 injection step. Consequently, the crystallinity of h-BN can be improved by healing the defects through the iteration of the etching and regrowth process during the MOCVD growth when H_2 carrier gas is used.

In order to support the proposed process, the etching and regrowth, experimentally, the effect of the number of pulse cycle on the characteristics of the h-BN grown with H_2 carrier gas was investigated. Increasing the number of pulse cycle does not result in a remarkable increase in the thickness of the grown film, as shown in the XRR spectra in Fig. 6(a) due to the self-terminating effect.[18,19] Despite similar thickness of the films, however, there is a significant change in optical absorption spectra, as shown in Fig. 6(b). When pulse cycle is 10, absorption peak is at around 198 nm which may be related to the turbostatic BN layers or relatively thinner h-BN layer formed at the early stage of the h-BN growth. In addition, there is a shoulder at around 210 nm which is suppressed by increasing the numbers of pulse cycle. Finally, the h-BN film grown for 120 pulse cycles shows the same optical absorbance characteristics as discussed in Fig. 1(b). The improvement of the h-BN characteristics as the pulse cycle increases is in agreement with the prediction of the etching and regrowth process presented above.

In summary, we have synthesized few-layer h-BN films on sapphire substrate by MOCVD by using two different carrier gases, H_2 and N_2, in order to figure out the role of the carrier gas on the characteristics of the h-BN. We observed broader XPS spectra, more prominent shoulder peaks in NEXAFS spectrum, and much larger electrical conduction from the h-BN film grown with N_2 carrier gas in comparison with those from the h-BN grown with H_2 carrier gas, which indicates that more defects exist in the h-BN film when N_2 carrier gas is used. Therefore, it was concluded that H_2 has an advantage over N_2 as a carrier for h-BN MOCVD growth which is more effective etching and regrowth processes occurring under the pulsed source-injection mode. Defects in h-BN film can be healed by such etching and regrowth processes, as a result, the crystallinity is improved during the MOCVD growth when H_2 carrier gas is employed.

ACKNOWLEDGMENTS

This work was supported by Samsung Research Funding Center of Samsung Electronics under Project Number SRFC-MA1401-10.

[1] A. Pakdel, Y. Bando, and D. Golberg, Chem. Soc. Rev. **43**, 934–959 (2014).
[2] A. Lipp, K. A. Schwetz, and K. Hunold, J. Eur. Ceram. Soc. **5**, 3–9 (1989).
[3] A. Gupta, T. Sakthivel, and S. Seal, Prog, Mater Sci. **73**, 44–126 (2015).

[4] Y. Kubota, K. Watanabe, O. Tsuda, and T. Taniguchi, Science **317**, 932–934 (2007).
[5] K. Watanabe, T. Taniguchi, and H. Kanda, Nat. Mater. **3**, 404–409 (2004).
[6] G. Cassabois, P. Valvin, and B. Gil, Nat. Photon. **10**, 262–266 (2016).
[7] L. Song, L. Ci, H. Lu, P. B. Sorokin, C. Jin, J. Ni, A. G. Kvashnin, D. G. Kvashnin, J. Lou, B. I. Yakobson, and P. M. Ajayan, Nano Lett. **10**, 3209–3215 (2010).
[8] C. R. Dean, A. F. Young, I. Meric, C. Lee, L. Wang, S. Sorgenfrei, K. Watanabe, T. Taniguchi, P. Kim, K. L. Shepard, and J. Hone, Nat. Nanotech. **5**, 722–726 (2010).
[9] K. K. Kim, A. Hsu, X. Jia, S. M. Kim, Y. Shi, M. Dresselhaus, T. Palacios, and J. Kong, ACS Nano **6**, 8583–8590 (2012).
[10] S. K. Jang, J. Youn, Y. J. Song, and S. Lee, Sci. Rep. **6**, 30449 (2016).
[11] Z. Liu, Y. Gong, W. Zhou, L. Ma, J. Yu, J. C. Idrobo, J. Jung, A. H. MacDonald, R. Vajtai, J. Lou, and P. M. Ajayan, Nat. Commun. **4**, 2541 (2013).
[12] R. Dahal, J. Li, S. Majety, B. N. Pantha, X. K. Cao, J. Y. Lin, and H. X. Jiang, Appl. Phys. Lett. **98**, 211110 (2011).
[13] S. Majety, X. K. Cao, J. Li, R. Dahal, J. Y. Lin, and H. X. Jiang, Appl. Phys. Lett. **101**, 051110 (2012).
[14] X. Z. Du, J. Li, J. Y. Lin, and H. X. Jiang, Appl. Phys. Lett. **108**, 052106 (2016).
[15] Y. Kobayashi and T. Akasaka, J. Cryst. Growth **310**, 5044–5047 (2008).
[16] Y. Kobayashi, C.-L. Tsai, and T. Akasaka, Phys. Status Solidi C **7**, 1906–1908 (2010).
[17] Y. Kobayashi, K. Kumakura, T. Akasaka, and T. Makimoto, Nature **484**, 223–227 (2012).
[18] Q. S. Paduano, M. Snure, J. Bondy, and T. W. C. Zens, Appl. Phys. Expr. **7**, 071004 (2014).
[19] Q. Paduano, M. Snure, D. Weyburne, A. Kiefer, G. Siegel, and J. Hu, J. Cryst. Growth **449**, 148–155 (2016).
[20] S. Caneva, R. S. Weatherup, B. C. Bayer, R. Blume, A. Cabrero-Vilatela, P. Braeuninger-Weimer, M. Martin, R. Wang, C. Baehtz, R. Schloegl, J. C. Meyer, and S. Hofmann, Nano Lett. **16**, 1250–1261 (2016).
[21] Y. Stehle, H. M. Meyer III, R. R. Unocic, M. Kidder, G. Polizos, P. G. Datskos, R. Jackson, S. N. Smirnov, and I. V. Vlassiouk, Chem. Mater. **27**, 8041–8047 (2015).
[22] M. Chubarov, H. Pedersen, H. Högberg, J. Jensen, and A. Henry, Cryst. Growth Des. **12**, 3215–3220 (2012).
[23] K. Nose, H. S. Yang, H. Oba, and T. Yoshida, Diamond Relat. Mater. **14**, 1960–1963 (2005).
[24] H. J. Kim, S. Choi, D. Yoo, J.-H. Ryou, R. D. Dupuis, R. F. Dalmau, P. Lu, and Z. Sitar, Appl. Phys. Lett. **93**, 022103 (2008).
[25] H. X. Jiang and J. Y. Lin, ECS J. Solid State Sci. Technol. **6**, Q3012–Q3021 (2017).
[26] J. C. Koepke, J. D. Wood, Y. Chen, S. W. Schmucker, X. Liu, N. N. Chang, L. Nienhaus, J. W. Do, E. A. Carrion, J. Hewaparakrama, A. Rangarajan, I. Datye, R. Mehta, R. T. Haasch, M. Gruebele, G. S. Girolami, E. Pop, and J. W. Lyding, Chem. Mater. **28**, 4169–4179 (2016).
[27] T. I. T. Okpalugo, P. Papakonstantinou, H. Murphy, J. McLaughlin, and N. M. D. Brown, Carbon **43**, 153–161 (2005).
[28] I. Jiménez, A. F. Jankowski, L. J. Terminello, D. G. J. Sutherland, J. A. Carlisle, G. L. Doll, W. M. Tong, D. K. Shuh, and F. J. Himpsel, Phys. Rev. B **55**, 12025 (1997).
[29] R. Franke, S. Bender, J. Hormes, A. A. Pavlychev, and N. G. Fominych, Chem. Phys. **216**, 243–257 (1997).
[30] A. B. Preobrajenski, A. S. Vinogradov, and N. Mårtensson, "Ni $3d$-BN π hybridization at the h-BN/Ni(111) interface observed with core-level spectroscopies," Phys. Rev. B **70**, 165404 (2004).
[31] L. A. Coldren and S. W. Corzine, *Diode Lasers and Photonic Integrated Circuits* (Wiley-VCH, New York, 1995).
[32] J. Stöhr and D. A. Outka, Phys. Rev. B **36**, 7891–7905 (1987).
[33] F.-C. Chiu, Adv. Mater. Sci. Eng. **2014**, 578168 (2014).
[34] W. Orellana and H. Chacham, Phys. Rev. B **63**, 125205 (2001).
[35] D. D. Koleske, A. E. Wickenden, R. L. Henry, J. C. Culbertson, and M. E. Twigg, J. Cryst. Growth **223**, 466–483 (2001).
[36] M. A. Mastro, O. M. Kryliouk, M. D. Reed, T. J. Anderson, A. Davydov, and A. Shapiro, Phys. State Solidi A **188**, 467–471 (2001).